Flow Structure of the Solids in a Three-Dimensional Liquid Fluidized Bed

ARTICLE *in* INDUSTRIAL & ENGINEERING CHEMISTRY RESEARCH · NOVEMBER 1997

Impact Factor: 2.59 · DOI: 10.1021/ie970161k

4 AUTHORS, INCLUDING:

Faïçal Larachi
Laval University
315 PUBLICATIONS **4,632** CITATIONS
SEE PROFILE

Miryan C. Cassanello
University of Buenos Aires
67 PUBLICATIONS **581** CITATIONS
SEE PROFILE

Jamal Chaouki
Polytechnique Montréal
275 PUBLICATIONS **3,590** CITATIONS
SEE PROFILE

Flow Structure of the Solids in a Three-Dimensional Liquid Fluidized Bed

Karim Kiared,[†] Faïçal Larachi,*[,‡] Miryan Cassanello,[§] and Jamal Chaouki[†]

Biopro Research Center, Department of Chemical Engineering, Ecole Polytechnique de Montréal, P.O. Box 6079, Station "Centre-Ville", Montréal, Québec, Canada H3C 3A7, Department of Chemical Engineering & CERPIC, Laval University, Québec, Canada G1K 7P4, and PINMATE, Departamento Industrias FCEyN, Universidad de Buenos Aires, 1428 Buenos Aires, Argentina

The motion of solids in a cylindrical liquid fluidized bed was experimentally characterized by means of a noninvasive radioactive particle tracking technique (RPT) for two monosized bed inventories, spherical glass beads (3 mm GB, density = 2500 kg/m^3) and nonspherical poly(vinyl chloride) particles (5.5 mm PVC, density = 1300 kg/m^3). RPT-monitoring of a single radioactive solid tracer mimicking faithfully the characteristics of the solids revealed the detailed solids flow features by determining the tracer instantaneous 3-D Lagrangian trajectory and then its local instantaneous velocities. Transverse solids dispersion coefficients were an order of magnitude lower than their axial counterpart. Time, longitudinal, and circumferential averaging of local velocities in the fully developed region of the fluidized bed revealed a weak gulf streaming characterized by axial velocities positive (respectively negative) in the core and negative (respectively positive) near the vessel walls for the GBs (respectively for the PVCs). The measured mean circumferential ensemble-averaged radial velocity was essentially zero in the fully developed region. The solids flow turbulence field was anisotropic, but the less dense the particles, the closer to isotropy was the solids flow. Computed shear stress profiles showed that PVC particles exhibited a higher shear stress than GB particles. The dynamic solids flow structure inside a 3-D liquid fluidized bed can be viewed as a core-annulus structure with axially-dispersed plug-flow and radial dispersion in each of the upward and downward zones.

Introduction

Relatively few experimental studies in liquid fluidization focused on the kinematics of the individual particles. In most of them, cinematography and photography techniques were the traditional tools of investigation, in which use was made of optically compatible seeds matching the liquid refractive index to track the motion of tracers in 2-D or 3-D liquid fluidization geometries. Handley et al. (1966) and Volpicelli et al. (1966) studied the particle movements in monolayer fluidized beds. Depending on the distributor design, two types of flow patterns were identified: (i) a uniform fluidization where particle motion was random and homogeneous and (ii) a nonuniform fluidization characterized by a bulk recirculation or gulf streaming of the solids. The particle motion was anisotropic, and a ratio of about 2 between vertical and horizontal root-mean-square velocities was reported. Handley et al. (1966) found that turbulent particle velocity components passed through a maximum at some voidage less than 0.70 and attributed the particle turbulent motion to random interchange between rising channels of fluid and falling streams of solids. Hanratty et al. (1956) applied the statistical theory of turbulence to study the hydrodynamics of liquid fluidized beds. The turbulence intensities calculated were invariant axially, indicating a certain homogeneity along the bed axis. The anisotropy in the solids flow was only mentioned without making a difference between axial and radial turbulence intensities. Carlos and Richardson (1968) and Latif and Richardson (1972) noted the formation of a clockwise solids bulk flow for glass particle beds, with particles rising in the bed core region and moving downward close to the vessel walls. The strength of the recirculation pattern was found to diminish toward the bed top. Although both studies were more quantitative than previous ones, due to very low statistics the accuracy of the reported measurements was poor and of limited value for modeling purposes. Kmieć (1978) studied the mechanics of particles in terms of structure and velocity. Although his results showed lot of scatter due to poor statistical events, his work confirmed the presence of a solids bulk flow and the anisotropic character of the particle velocities in the vertical and horizontal directions. Gbavčić et al. (1990) tracked the motion of glass beads in a bidimensional liquid fluidized bed and found that the degree of anisotropy of solids motion increased with increasing liquid velocity. Recently, Bascoul et al. (1993) devised a very simple radioactive particle tracking technique to measure semiqualitatively particle motion in monolayer fluidized beds. For sufficiently tall beds and consistent with the above bulk recirculation pattern, the solids flow structure was viewed as two countercurrent vertical zones within each of which the solids motion was well described by an axially dispersed plug flow. These two zones were relatively hermetic and characterized by a limited horizontal exchange of solids; the pattern proposed for solids displacements corresponded to combined convection−dispersion motion mechanisms. Limtrakul (1996) used a radioactive particle tracking technique (CARPT) to measure the 1-D radial distributions of axial and radial average velocities and axial and radial turbulent velocities in the fully developed region of a monolayer liquid fluidized bed.

* Author to whom correspondence is addressed. Phone: (418)-656-3566. Fax: (418)-656-5993. E-mail: flarachi@gch.ulaval.ca.

[†] Ecole Polytechnique de Montréal. Phone: (514)-340-4711-4034. Fax: (514)-340-4159. E-mail: jchaouki@mailsrv.polymtl.ca and kiared@chimie.polymtl.ca.

[‡] Laval University.

[§] Universidad de Buenos Aires. Phone: (54-1)-781-5021/29 ext. 360. Fax: (54-1)-784-0208. E-mail: miryan@ferbat.uba.ar.

S0888-5885(97)00161-9 CCC: $14.00

Water fluidizing velocities between 2.5 and 13 cm/s were explored in the case of 3 mm glass beads and 3 mm acetate beads (density = 1300 kg/m^3) in two columns of different diameters fitted with perforated plates as liquid distributors. From her work it appeared that, irrespective of the bed inventory tested, the solids flow exhibited a bulk recirculation pattern with particles ascending in the core from the column center to the flow reversal radius and descending from the flow reversal radius to the wall. Analysis of the turbulent velocities revealed that the motion of the high-density particles (glass beads) was close to isotropy, while that of the low-density particles (acetate beads) departed from isotropy with axial root-mean-square velocities in excess of their radial counterpart.

Low statistics in the measured events, tedious manipulation, experimental difficulties associated with refractive-index mismatch, and nonappropriateness for opaque flows are known as inherent limitations of the optical measuring techniques. Therefore, except for Limtrakul's CARPT investigations (Limtrakul, 1996), all or most of the information acquired until recently on the solids motion in monolayer liquid fluidized beds may be regarded as more qualitative than quantitative and thus are not easily amenable for utilization in predictive models of solids flow such as in CFD modeling. As perceived from the latest paper on liquid fluidization by Di Felice (1995), there is an evident paucity of reliable quantitative data on the radial distributions of particle radial and axial velocities, root-mean-square velocities, turbulent intensities, shear stress and transverse dispersion coefficients, etc., in monolayer liquid fluidized-bed reactors.

The scope of the present experimental study was to apply a noninvasive radioactive particle tracking, similar to CARPT, to accurately measure local and global solids flows in a 3-D monolayer liquid fluidized bed. Measured 3-D trajectories of the solids were discussed in both Lagrangian and Eulerian frameworks. The dispersion coefficients in x, y, and z directions, the time-averaged velocity field, and the flow properties belonging to the fully developed region, e.g., radial and axial mean velocities, radial and axial turbulent velocities, and shear stress and anisotropy coefficient, were derived.

Fluidized-Bed and Particle Tracking Facilities

The results presented here were obtained in a Plexiglas column of 100 mm inner diameter and 1500 mm height. A simplified flow diagram of the experimental setup is shown in Figure 1a,b. The bottom of the fluidized bed was fitted with a liquid distributor comprising a conical bed packed with 5 mm glass beads, which acts as a calming zone, a cylindrical bed packed with 2 mm glass beads, and a perforated plate sandwiched in between. The plate, with a fractional open area of 5.5%, contained holes 0.74 mm in diameter arranged in a triangular pitch and spaced every 2 mm. Fine stainless steel screens were provided at each side of the column to circumvent entrainment of the fluidized particles or their contact with the distributor particles. The fluidized particles were 3 mm spherical glass beads (GB) with a density of 2500 kg/m^3 and 5.5 mm nonspherical poly(vinyl chloride) (PVC) hexagonal particles with a density of 1300 kg/m^3. The mass of particles introduced in the column was 3.8 and 0.8 kg for GB and PVC, respectively, giving 320 and 180 mm defluidized bed heights. The liquid, which was tap water, was delivered to the column by a Moyno pump from a feed tank. A set of calibrated rotameters measured the liquid flowrate. An expanded bed height to diameter ratio was kept around 5, which corresponded to bed porosities of 0.52 and 0.83 for GB and PVC, respectively. The minimum fluidization velocities were 3.2 and 1.8 cm/s for GB and PVC, respectively.

The instantaneous tracer particle trajectories in the liquid fluidized bed were measured with the radioactive particle tracking system (RPT), which was used earlier for the solids motion measurements in gas-spouted beds (Roy et al., 1994), binary liquid fluidized beds (Larachi et al., 1995), three-phase fluidized beds (Larachi et al., 1996), and circulating fluidized beds (Godfroy et al., 1996). A similar tracking system had already been applied to liquid and three-phase fluidized beds by Limtrakul (1996) and to bubble columns by Devanathan et al. (1990) and Degaleesan et al. (1996). Radio-labeled tracers, obtained through neutron radiative capture by ^{45}Sc, were irradiated to reach an activity level of 50 μCi. The resulting ^{46}Sc isotopes underwent β decay and emitted a pair of γ-rays of nearly 1 MeV. To ensure a perfect ability to trace the phases of interest, a glass bead and a PVC particle were picked up from the actual solids inventories. They were filled with the material to be activated and were then secured by a seal before introduction in the fluidized bed. An array of eight (3 in. $\times$ 3 in.) uncollimated and unshielded NaI(Tl) scintillation detectors, arranged around the fluidized bed (Figure 1a), was used to monitor the count rates of the γ-rays emitted from the wandering tracers. These count rates were converted into instantaneous Lagrangian trajectories using an appropriate triangulation procedure. Full details on the system calibration and triangulation procedure are thoroughly described elsewhere (Larachi et al., 1994).

Results and Discussion

The discussion hereafter on the particle instantaneous movements will be subdivided into two parts as follows: particle trajectory and particle dispersion coefficients in the Solids Kinematics section and mean flow pattern, one-dimensional profiles of axial and radial velocity components, one-dimensional turbulence parameters, and solids flux balance in the Mean Solids Flow Field Characteristics section.

Solids Kinematics. *Particle Trajectory.* Typical three-dimensional tracks of the 5.5 mm PVC and the 3 mm GB tracers in the fluidized bed are shown in Figure 2a−f for two liquid velocities, respectively 0.058 and 0.065 m/s. The horizontal locations x and y (in mm) and the vertical location z (in mm) of both tracers in the bed are plotted as a function of elapsed time. Sample histories depicting only 165 s of successive positions were taken from runs lasting up to 10 h. For all the experiments, the elapsed time between two successive samples was fixed at 160 ms. The range of transversal motion was bounded by the end walls of the cylindrical column ($\pm$50 mm), as indicated by the horizontal lines drawn in Figure 2a−d. The range of vertical motion was bounded by the distributor ($z = 0$) and the expanded bed upper level ($z \approx 450$ mm), as indicated by the horizontal dashed lines in Figure 2e,f.

Horizontally, particles were observed to undergo saw-toothed displacements and exhibited many short loops corresponding to no specific direction (Figure 2a−d). Vertices on such loops corresponded to deflections brought about by tracer−particle or tracer−wall colli-

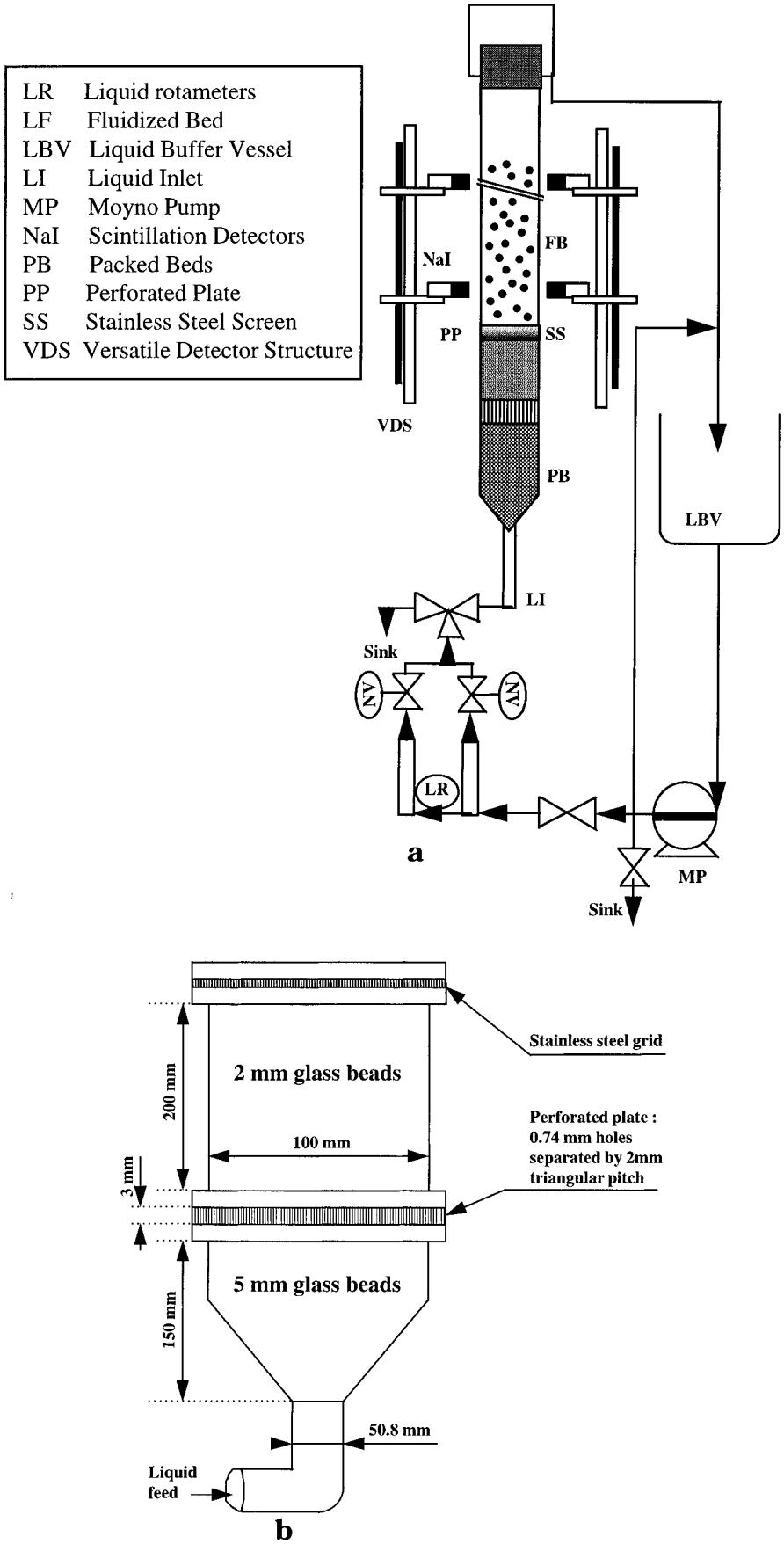

Figure 1. Schematic of (a) fluidization setup and RPT detection system and (b) packed-bed perforated plate distributor.

sions and by fluid−tracer interactions. Although the bed of PVC particles was more expanded ($\epsilon = 0.83$) than the bed of glass beads ($\epsilon = 0.52$), the less dense tracer (i.e., PVC) underwent more frequent deflections than the heavier tracer (i.e., glass bead); see Figure 2a,b. However, hindrance within the bed of glass beads did not impede the GB tracer to wander around the whole horizontal section, as illustrated in Figure 2b,d. More-

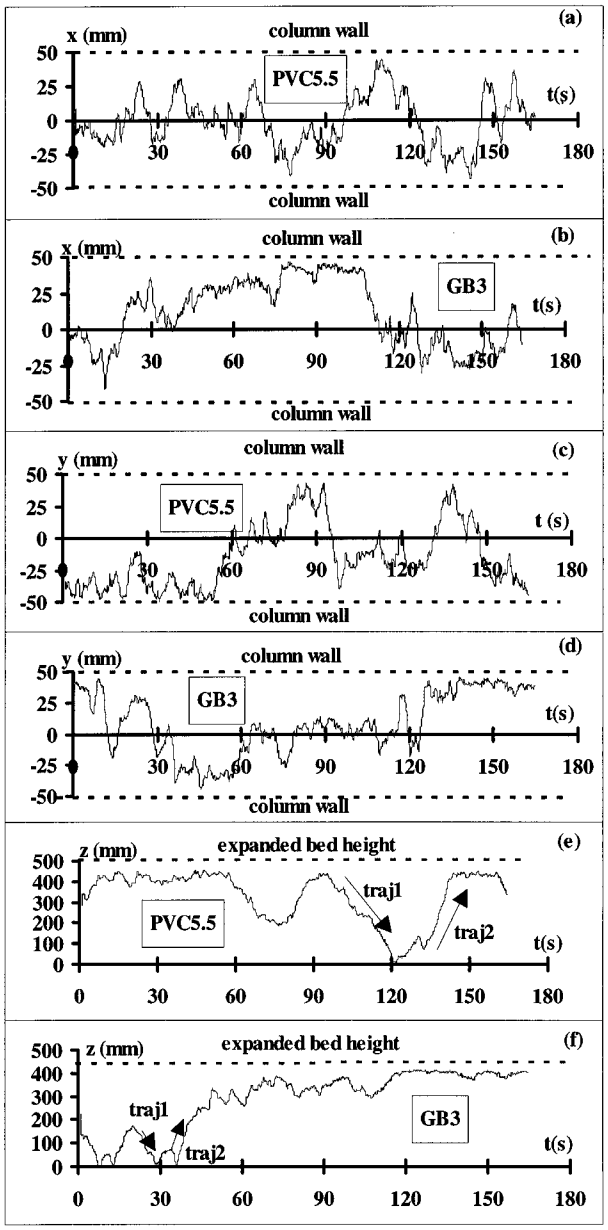

Figure 2. Displacement-time charts showing the variations in *x*, *y*, and *z* directions of the tracer over 165 s for the PVC and GB beds (sampling period = 160 ms). Glass beads: $u_L = 0.065$ m/s; $\epsilon = 0.52$, $d_p = 3$ mm, $D_c = 10$ cm. PVC particles: $u_L = 0.058$ m/s; $\epsilon = 0.83$, $d_p = 5.5$ mm, $D_c = 10$ cm.

over, a study of the time-averaged radial particle velocity profiles (see the next section) did not reveal significant radial advective flow. This was in favor of a Brownian-like or a dispersion-type mechanism which might solely account for the transverse transport of solids in liquid fluidized beds. Using a rescaled range fractal analysis (Mandelbrot and Wallis, 1969), Cassanello et al. (1995) determined the so-called Hurst exponents for both *x* and *y* trajectories which were found to be close to $^1/_2$ for the two experiments analyzed in this work. This indeed confirmed that the transverse solids displacements were characterized by Brownian dispersion and could be described by Fick's law with constant dispersion coefficients for *x* and *y* directions.

Axially, both PVC and GB tracers displayed ascending and descending convective motion patterns whereon small-amplitude fluctuations were superimposed (Figure 2e,f). The same figures show that both tracers spent nonnegligible times floating close to the free surface of

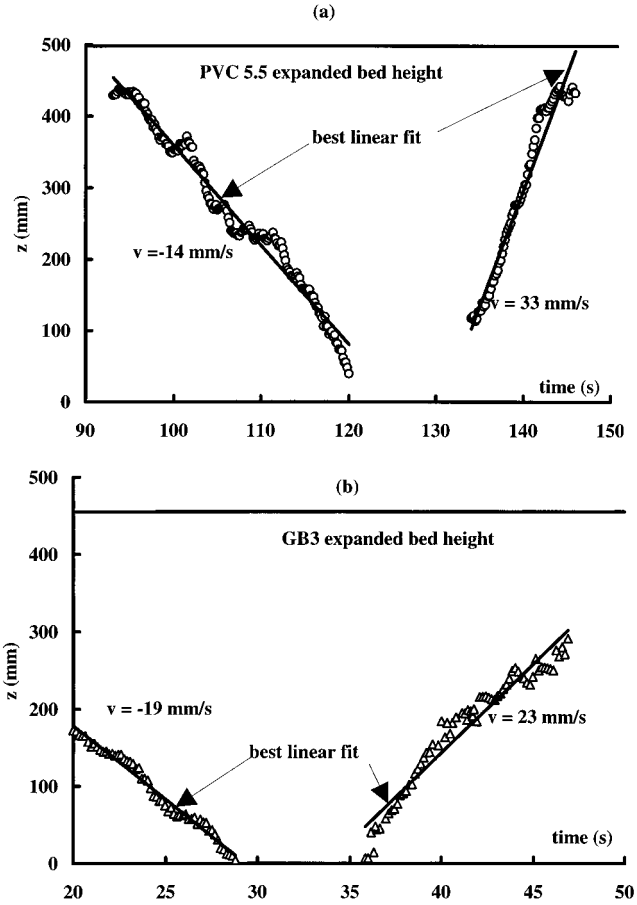

Figure 3. Zoom of a rising (traj1) and a descending (traj2) portion from the vertical movements of the PVC tracer (a) and the glass bead tracer (b), together with the best regression lines and the corresponding slopes (or velocities).

the beds and made short movements in different horizontal directions (Figure 2a−d) until they reached a downflowing region either near the wall or in the bed core, where they initiated a slow descent. Zooming in some selected ascending and descending portions of the tracers' vertical movements (traj1 and traj2 in Figure 2e,f) shows that each vertical displacement proceeded at almost constant axial velocity d*z*/d*t*, as demonstrated by the best linear fits of the *z* versus time curves shown in Figure 3a,b. As a general rule, the ratio of liquid velocity to particle axial velocity was close to 5 and agreed well with the results reported by Carlos and Richardson (1968), Gbavčić et al. (1990), and Bascoul et al. (1993). A pair of successive rising and descending portions formed unsymmetrical peaks with ascent and descent of different lengths (Figure 2e,f). Moreover, some vertical movements extended uninterruptedly from the bed free surface to the distributor and *vice versa*. It is precluded that such long amplitude movements were the result of a dispersive motion alone but were likely due to the existence of a weak overall recirculation pattern of the solids. Although considerable precautions were taken in the design of the liquid distributor in order to ensure as uniform as possible liquid feed, a weak gulf streaming was always present, as will be shown later.

Particle Dispersion Coefficients. The particle dispersion coefficients in the three directions were computed as the time derivatives of the corresponding Lagrangian particle mean-square displacements (Monin and Yaglom, 1971), as indicated by eq 3 in Table 1. By computing the solids particle dispersion coefficients in

Table 1. Flow Quantities Calculated from RPT Data

Lagrangian

projections of excess displacements of the tracer released from a reference point $\Xi_0(x_0,y_0,z_0)$:

$$X(\Xi_0,t) = x(t) - x_0, \quad \text{same for } y \text{ and } z \text{ directions} \tag{1}$$

ensemble-averaged instantaneous displacements:

$$\langle\overline{X(\Xi_0,t)}\rangle = \frac{1}{P}\sum_{j=1}^{P} X_j(\Xi_0,t), \quad \text{same for } y \text{ and } z \text{ directions} \tag{2}$$

mean-square displacements and dispersion coefficients:

$$\langle\overline{X^2(\Xi_0,t)}\rangle = \frac{1}{P}\sum_{j=1}^{P}(X_j(\Xi_0,t) - \langle\overline{X(\Xi_0,t)}\rangle)^2, \quad \text{same for } y \text{ and } z \text{ directions}$$
$$D_x(\Xi_0,t) = \frac{\mathrm{d}}{2\,\mathrm{d}t}\langle\overline{X^2(\Xi_0,t)}\rangle, \quad \text{same for } y \text{ and } z \text{ directions} \tag{3}$$

Eulerian

time:

$$\begin{array}{ll} t_i & \text{location } r_i, \theta_i, z_i \\ t_i + T & \text{location } r_{i+1}, \theta_{i+1}, z_{i+1} \end{array}$$

coordinates of midpoint:

$$\begin{pmatrix} r_\mathrm{m} \\ \theta_\mathrm{m} \\ z_\mathrm{m} \end{pmatrix} = \begin{pmatrix} \sqrt{{x_\mathrm{m}}^2 + {y_\mathrm{m}}^2} \\ \arctan\left(\dfrac{y_\mathrm{m}}{x_\mathrm{m}}\right) \\ z_\mathrm{m} \end{pmatrix} \tag{4}$$

local instantaneous velocity:

$$u(r_\mathrm{m},\theta_\mathrm{m},z_\mathrm{m}) = \begin{pmatrix} u_r \\ u_\theta \\ u_z \end{pmatrix} = \begin{pmatrix} (r_{i+1} - r_i)/T \\ r_\mathrm{m}(\theta_{i+1} - \theta_i)/T \\ (z_{i+1} - z_i)/T \end{pmatrix} \tag{5}$$

local time (ensemble)-averaged velocity:

$$\langle\mathbf{u}(r_\mathrm{m},\theta_\mathrm{m},z_\mathrm{m})\rangle = \frac{1}{P}\sum_{j=1}^{P}\mathbf{u}_j(r_\mathrm{m},\theta_\mathrm{m},z_\mathrm{m}) \tag{6}$$

eulerian fluctuating velocity:

$$\mathbf{u}'(r_\mathrm{m},\theta_\mathrm{m},z_\mathrm{m}) = \mathbf{u}(r_\mathrm{m},\theta_\mathrm{m},z_\mathrm{m}) - \langle\mathbf{u}(r_\mathrm{m},\theta_\mathrm{m},z_\mathrm{m})\rangle \tag{7}$$

correlation between fluctuating velocities:

$$\langle u_k' u_l'\rangle = \frac{\displaystyle\int_{z_\mathrm{low}}^{z_\mathrm{high}}\int_0^{2\pi}\sum_{j=1}^{P} u_{kj}'(r_\mathrm{m},\theta_\mathrm{m},z_\mathrm{m})\, u_{lj}'(r_\mathrm{m},\theta_\mathrm{m},z_\mathrm{m})\,\mathrm{d}\theta\,\mathrm{d}z}{\displaystyle\int_{z_\mathrm{low}}^{z_\mathrm{high}}\int_0^{2\pi} P\,\mathrm{d}\theta\,\mathrm{d}z} \tag{8}$$

azimuthally and axially averaged time (ensemble)-averaged velocity:

$$\mathbf{U}(r_\mathrm{m}) = \frac{\displaystyle\int_{z_\mathrm{low}}^{z_\mathrm{high}}\int_0^{2\pi}\langle\mathbf{u}(r_\mathrm{m},\theta_\mathrm{m},z_\mathrm{m})\rangle P(r_\mathrm{m},\theta_\mathrm{m},z_\mathrm{m})\,\mathrm{d}\theta\,\mathrm{d}z}{\displaystyle\int_{z_\mathrm{low}}^{z_\mathrm{high}}\int_0^{2\pi} P\,\mathrm{d}\theta\,\mathrm{d}z} \tag{9}$$

turbulence intensities:

$$I_k = \frac{\sqrt{\langle {u_k}'^2\rangle}}{U_z(r_\mathrm{m})} \tag{10}$$

anisotropy coefficient:

$$\mathrm{AC} = \sqrt{\frac{\langle {u_k}'^2\rangle}{\langle {u_l}'^2\rangle}} \tag{11}$$

volumetric solids flow rate in the central core region:

$$\dot{Q}_\mathrm{c} = \int_0^{r_\mathrm{FR}} 2\pi\epsilon_\mathrm{S}(r)\, U_z r\,\mathrm{d}r \tag{12}$$

volumetric solids flow rate in the sidewall region:

$$\dot{Q}_\mathrm{sw} = \int_{r_\mathrm{FR}}^{r_\mathrm{w}} 2\pi\epsilon_\mathrm{S}(r)\, U_z r\,\mathrm{d}r \tag{13}$$

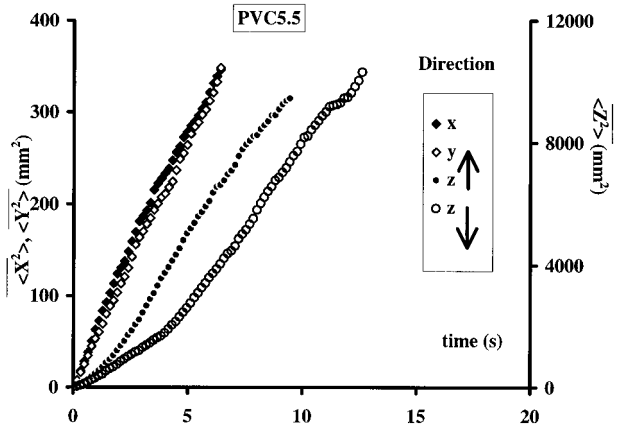

Figure 4. Time dependence of the mean-square displacements of the PVC tracer in x, y, and z (up and down) directions. u_L = 0.058 m/s; $\epsilon = 0.83$, $d_p = 5.5$ mm, $D_c = 10$ cm.

this way, we assumed (i) anisotropic but homogeneous solids flow field in each of the three spatial directions and (ii) marginal effect of the velocity gradient of the axial advective Eulerian mean velocity. In sheared flows, Degaleesan (1997) and Degaleesan et al. (1997) showed indeed that the incorporation of the velocity gradient correction is marginal for low fluid throughputs. Axial dispersion coefficients of solids in liquid fluidized beds were also determined by Limtrakul (1996), assuming homogeneous turbulence and gradientless streamwise velocity.

Figure 4 shows, in the case of the PVC tracer, the time evolution of the mean-square displacements in the directions x, y, and z. These profiles were obtained by averaging over 20 different release locations inside the bed. Since a gross recirculation pattern for the solids was noticed, a distinction was made between ascending and descending trajectories in order to quantify the axial dispersion coefficient in each of the ascending and descending regions. The average D_x, D_y, and D_z values for the entire bed, calculated for the glass beads and the PVC particles, are shown in Table 2. Horizontal dispersion coefficients in x and y directions were almost identical and independent of the particle size and density; however, they were an order of magnitude lower than the axial dispersion coefficient. Limtrakul's (1996) axial dispersion coefficients measured by CARPT for 3 mm GB were also given in the table, where it is seen that they compare quite well with our data for close water fluidizing velocities. For comparison, some effective axial dispersion coefficients available from the literature were also provided in Table 2.

Mean Solids Flow Field Characteristics. So far the Lagrangian analysis provided a refined description of the three-dimensional and instantaneous motion of the tracer in the fluidized bed. In what follows, a complementary description using the Eulerian framework is given for quantitatively representing the time-averaged solids flow structure.

Mean Flow Pattern. By assuming that circumferential symmetry existed, the mean velocity pattern was obtained by dividing the bed into 240 $r-z$ pixels (8 radii $\times$ 30 axial cuts) and ascribing the computed radial and axial velocity components to each pixel. Actually in 3-D a pixel corresponds to an annular volume of height Δz, thickness Δr, and radius r, which is located at height z above the distributor. Because two successive positions were used for each velocity vector, the coordinates of midpoint were used in assigning each velocity vector to the pixel of closest centroid. In a typical experiment with a total of about 200 000 individual velocity components, the average number of events per pixel was 800.

The developments of axial and radial velocities of PVC tracer over the entire fluidized bed are illustrated by the $r-z$ contour plots of U_z and U_r in Figure 5a,b, respectively. The contour plots are based on a continuous gray level scale, and only half of the bed is shown, the column axis being on the left. Two regions can be distinguished from Figure 5a: a central region where the solids circulated predominantly downward and a wall region where they circulated predominantly upward. Near the bed entrance region, the radial solids flow was outward (positive radial velocities), while the PVC tracer exhibited the fastest descending motion (Figure 5a,b). The radial velocities were virtually zero (5 mm/s and less) throughout the major part of the bed, with the exception of the suspension-freeboard region where an inward flow was detected. This would suggest that the solids bulk flow was triggered by a pair of large toroidal recirculation cells filling the entire bed. The sense of rotation in these recirculation cells was anticlockwise. Analysis of the flow pattern for the bed of glass beads (not shown here) revealed two pairs of counter-rotating recirculation cells: small anticlockwise cells in the entry region and large clockwise cells in the bed upper region. Clockwise recirculation cells as those noted for the 3 mm glass beads were also in agreement with Limtrakul (1996) recirculation patterns observed via CARPT for 3 mm GB and by Latif and Richardson (1972) and Carlos and Richardson (1968) when testing beds of 8.9 and 6.2 mm glass beads, respectively.

1-D Radial Profiles of Axial and Radial Velocity Components. RPT enabled measuring the whole 3-D solids flow field including both end and fully developed regions. For columns with high aspect ratios, interest in the fully developed region (FDR) is important because (i) FDR represents the largest portion of the reactor and (ii) in FDR the time-averaged flow is axially invariant and circumferentially symmetrical to allow one-dimensional analysis and to support simple flow models. Such an analysis of flow data leads to compact data representations and easy interpretation by only considering radial variations of turbulent and time-averaged velocity components, shear stress, eddy diffusion coefficients, etc. The 1-D data reduction in the FDR was performed by time, circumferentially and longitudinally averaging the instantaneous particle velocities and the square and cross products of the fluctuating velocities. At each radial location r, the triple averaging was performed on a cylindrical shell of thickness Δr, at which elevations z_{low} and z_{high} delineated respectively the lower and upper limits of the FDR. Various Eulerian quantities that may be computed from the tracer trajectory for the 1-D analysis are shown in Table 1.

Figure 6 shows the 1-D radial profiles of axial and radial velocities for PVC and GB beds corresponding to the FDR. Consistent with the aforementioned recirculation patterns, GB particles (respectively PVC) rose (respectively descended) in the central region of the column and descended (respectively rose) close to vessel walls. The locus of the zero axial velocity, i.e., inversion region or flow reversal, occurred at a reduced radius $\zeta_{FR} \approx 0.7$. On an average basis, the flow reversal region roughly separates the particle upflow region from the particle downflow region. The particles rose faster in the upflow region (U_z up to 22 mm/s) than when they

Table 2. Solids Dispersion Coefficients $\times 10^6$ (m^2/s)[a]

particles	z-direction down	z-direction up	average	x-direction	y-direction	superficial liquid velocity (m/s)	reference
5.5 mm PVC	483[b]	426[b]	464[b]	28.3[b]	26.8[b]	0.058	this work
3 mm GB	459[b]	475[b]	460[b]	30.1[b]	28.3[b]	0.065	this work
3 mm GB			~500[b]			0.070	Limtrakul, 1996
3 mm GB			~3000[b]			0.100	Limtrakul, 1996
0.65 mm GB	83	78				0.055	Bascoul et al., 1993
2 mm GB			140			0.045	Juma and Richardson, 1983
3 mm GB			130			0.045	Juma and Richardson, 1983
3.1 mm GB			350				Al-Dibouni and Garside, 1979
3 mm GB			500			0.060	Kang et al., 1990

[a] Liquid = water. [b] Assuming homogeneous turbulence and gradientless streamwise velocity.

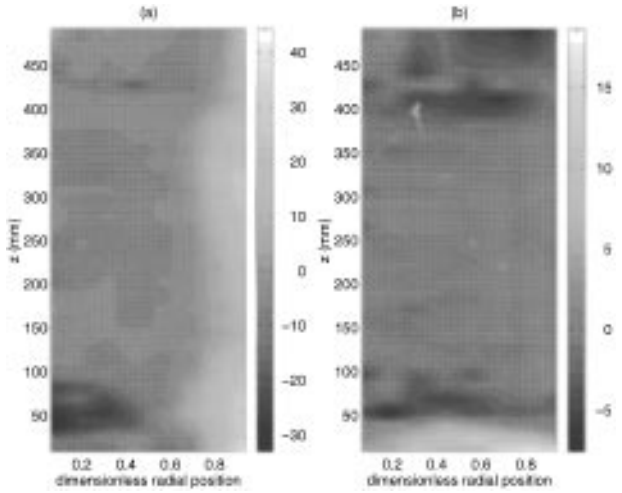

Figure 5. Contour plots in the $r-z$ frame of the PVC particle axial (a) and radial (b) mean velocities, $u_L = 0.058$ m/s, $\epsilon = 0.83$, $d_p = 5.5$ mm, $D_c = 10$ cm.

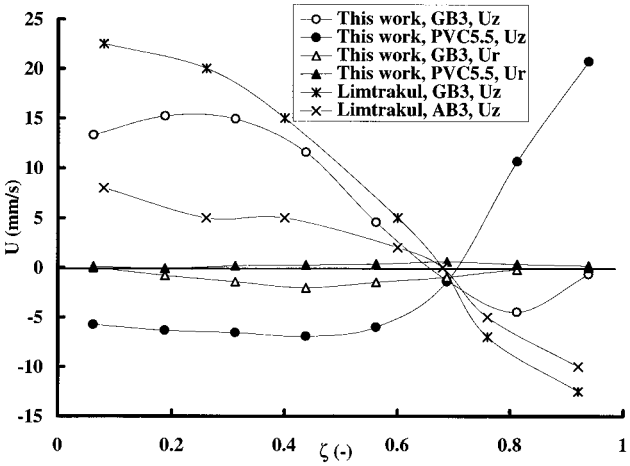

Figure 6. One-dimensional axial and radial particle velocity profiles in the fully developed region of the PVC, GB, and AB beds. This work: glass beads, $u_L = 0.065$ m/s, $\epsilon = 0.52$, $d_p = 3$ mm, $D_c = 10$ cm; PVC particles, $u_L = 0.058$ m/s, $\epsilon = 0.83$, $d_p = 5.5$ mm, $D_c = 10$ cm. Limtrakul's work (1996): glass beads, $u_L = 0.070$ m/s, $\epsilon = 0.44$, $d_p = 3$ mm, $D_c = 10$ cm; acetate beads (AB), $u_L = 0.070$ m/s, $\epsilon = 0.44$, $d_p = 3$ mm, $D_c = 14$ cm.

went down in the downflow region ($0 < U_z < -5$ mm/s). As argued by Bascoul et al. (1993), the difference between upward and downward velocities may be caused by a nonuniform radial distribution of porosity, with less void in the downflow region but more in the upflow region.

Obviously in the FDR and as confirmed by Figure 6, the mean local radial velocities were negligibly smaller compared to the axial velocities. This was consistent with Latif and Richardson's (1972) and Limtrakul's (1996) findings and the Bascoul et al. (1993) two-zone flow structure.

Figure 6 also shows a comparison with radial distributions of axial velocities, U_z, as measured by Limtrakul (1996) using CARPT. 3 mm GB and 3 mm acetate beads (AB3, density = 1300 kg/m^3) were water-fluidized at $u_L = 0.07$ m/s in a 100-mm i.d. column and a 140-mm i.d. column, respectively, leading to equal bed porosities ($\epsilon = 0.44$). From the figure it is seen that only for the glass beads the velocity profiles agreed qualitatively for both studies. Although the acetate beads tested by Limtrakul (1996) had a density equal to that of the PVC particles used in our study, the latter showed a quite peculiar velocity profile. There may be three reasons for that: (i) the distributor design, (ii) the shape of the low-density particles, and (iii) the bed porosities which were different from the two studies. It is well established that the influence of the distributor design is significant for low-density particles, whereas high-density particles tend to overwhelm the distributor hydrodynamic disturbances (Asif et al., 1992). Low-density particles are more distributor-sensitive than high-density particles. Also, nonsphericity of the particles appears to be influential. A previous study of binary liquid fluidized beds revealed indeed that nonspherical polypropylene extrudates (3.1 mm in size) mixed with 0.9 mm glass beads recirculated upward in the sidewalls and downward in the bed core region (Larachi et al., 1995). Finally, the porosity of the PVC5.5 bed ($\epsilon = 0.83$) was almost double that of the AB3 bed ($\epsilon = 0.44$), implying consequently very distinct expansion characteristics of the two beds (see Di Felice, 1995).

1-D Turbulence Parameters. Parts a–c of Figure 7 show the one-dimensional representation of the solids root-mean-square (rms) axial (u_z') and radial (u_r') velocities and shear stress ($\langle u_r' u_z \rangle$) versus dimensionless radius ζ for PVC and GB fluidized beds. Axial rms velocities can be as high as 30 mm/s and appeared to exceed the average axial velocities. Radial rms velocities far outweighed the average radial velocities to conclude that, in the plane transverse to the liquid flow, a dispersion-type mechanism solely accounted for solids motion. Axial and radial normal stresses ($u_r'^2$, $u_z'^2$) and shear stress ($\langle u_r' u_z' \rangle$) did not differ too much, and PVC particles exhibited slightly larger stresses than GB particles. Parts a and b of Figure 7 show for comparison u_z' and u_r' radial profiles measured by Limtrakul for the same conditions as those depicted in the previous section.

By defining a turbulence intensity parameter as the ratio between the local rms velocity and the corresponding average axial velocity (eq 10, Table 1), it was possible to assess the relative contribution of turbulent and advective movements along the radial coordinate.

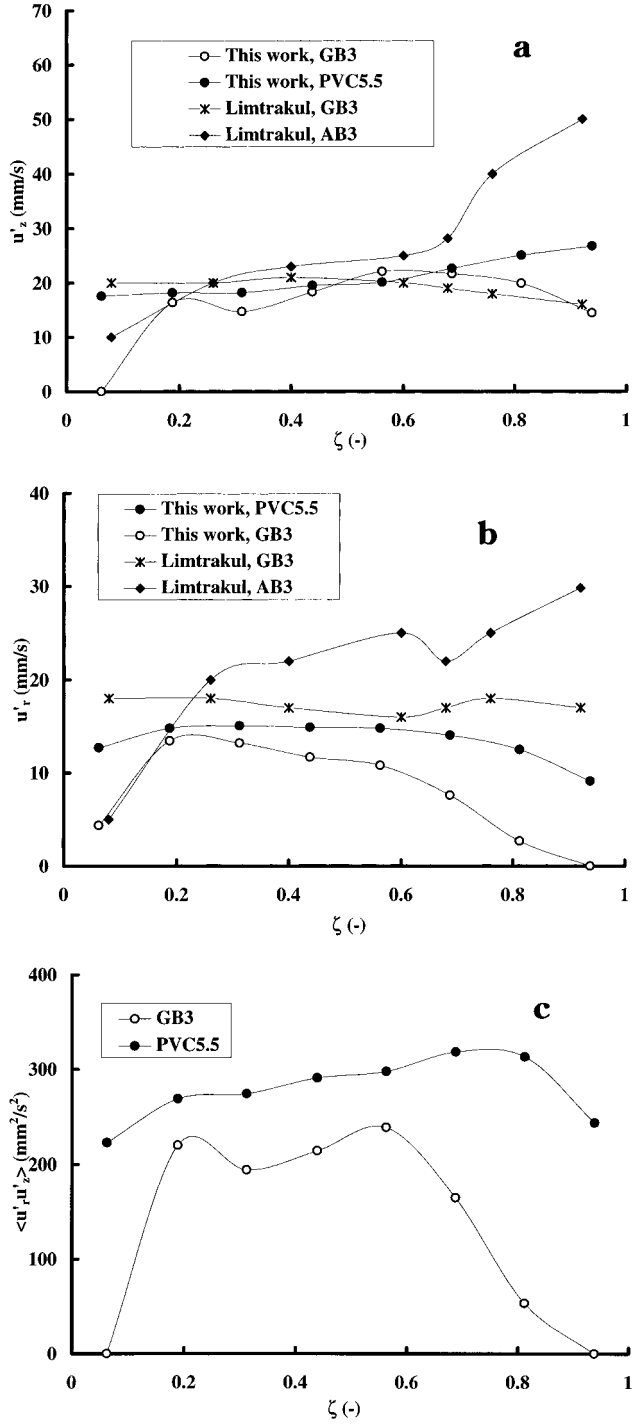

Figure 7. One-dimensional particle axial root-mean-square velocity (a), radial root-mean-square velocity (b), and shear stress (c) profiles in the fully developed region of the PVC, GB, and AB beds. This work: glass beads, $u_L = 0.065$ m/s, $\epsilon = 0.52$, $d_p = 3$ mm, $D_c = 10$ cm; PVC particles, $u_L = 0.058$ m/s, $\epsilon = 0.83$, $d_p = 5.5$ mm, $D_c = 10$ cm. Limtrakul's work (1996): glass beads, $u_L = 0.070$ m/s, $\epsilon = 0.44$, $d_p = 3$ mm, $D_c = 10$ cm; acetate beads (AB), $u_L = 0.070$ m/s, $\epsilon = 0.44$, $d_p = 3$ mm, $D_c = 14$ cm.

Hence, radial profiles of axial, I_z, and radial, I_r, turbulence intensities are shown in Figure 8a,b. Since the local average axial velocity was essentially zero at ζ_{FR} (flow reversal) location, the plotted profiles presented a discontinuity there. Except near ζ_{FR}, the PVC particles exhibited systematically larger turbulence intensities than the glass beads. Turbulence accounted for more than advection in the motion of PVC particles (a factor of 2 radially and a factor of 3 axially), whereas

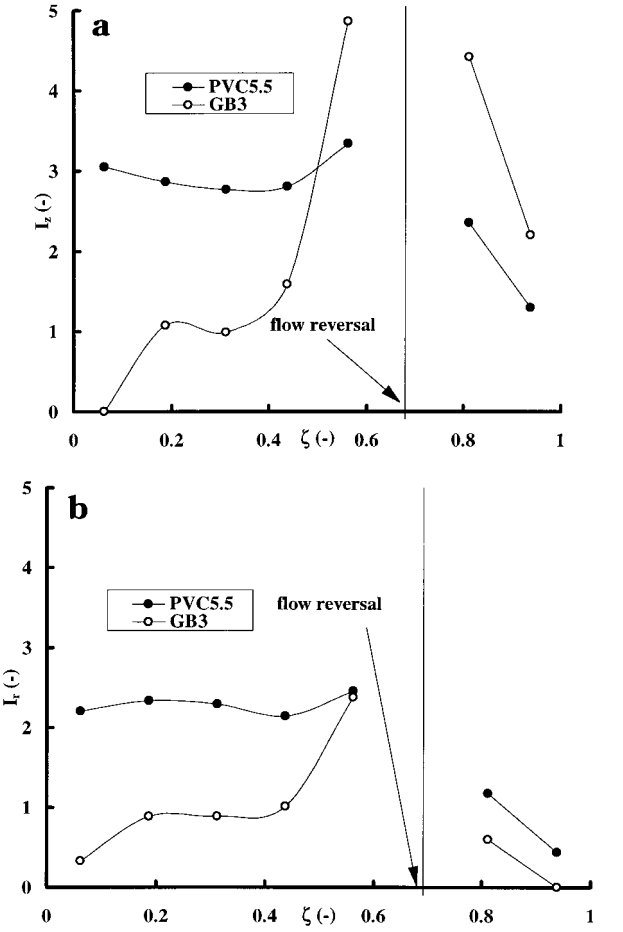

Figure 8. One-dimensional particle turbulence intensity profiles in axial (a) and radial (b) directions of the fully developed region of the PVC and GB beds. Glass beads: $u_L = 0.065$ m/s, $\epsilon = 0.52$, $d_p = 3$ mm, $D_c = 10$ cm. PVC particles: $u_L = 0.058$ m/s, $\epsilon = 0.83$, $d_p = 5.5$ mm, $D_c = 10$ cm.

for glass beads in the core region of the bed turbulent and advective contributions were comparable.

Solids turbulent motion was also described using an anisotropy coefficient AC (eq 11, Table 1), which compared turbulent motion axially to turbulent motion radially. For AC = 1, isotropy is fulfilled, while AC values departing from unity indicate flow anisotropy. AC versus ζ profiles for GB and PVC are presented in Figure 9. The maximum ratio reached by AC was 85% and occurred in the central region of the bed. For both bed inventories and as expected, AC steadily decreased toward the vessel walls. The PVC bed showed less anisotropy than the glass bead bed. For both particle types, the central region appeared to be closer to isotropy than the sidewall region.

Solids Flux Balance in the FDR. To satisfy the continuity equation in the FDR, the net solids volume flow rate should be identically zero at any height in the fluidized bed. Across any horizontal cross-sectional area, the difference between the average central advective solids volumetric flow rate, $\dot{Q}_c$ (eq 12, Table 1), and the sidewall advective solids volumetric flow rate, $\dot{Q}_{sw}$ (eq 13, Table 1), provides, in principle, an indication of the accuracy of the particle average velocity distributions. As there is no certainty that the average solids volume fraction distribution, $\epsilon_S(r)$, is constant along the radial coordinate, verification of the continuity equation is precluded unless the $\epsilon_S(r)$ profile is determined otherwise, e.g., measured by densitometry or tomography techniques. Only if we postulate that the number

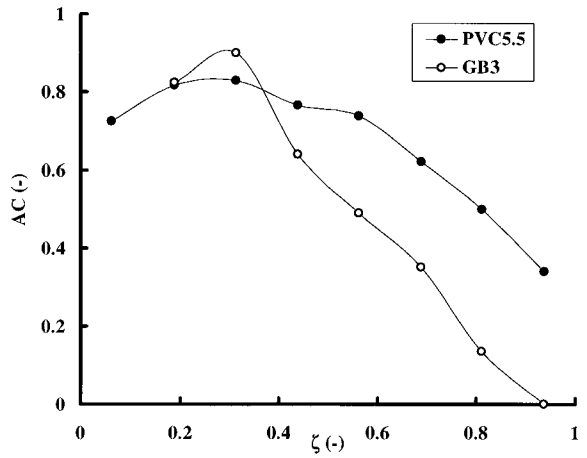

Figure 9. One-dimensional radial profile of anisotropy coefficient of the solids in the fully developed region of the PVC and GB beds. Glass beads: $u_L = 0.065$ m/s, $\epsilon = 0.52$, $d_p = 3$ mm, $D_c = 10$ cm. PVC particles: $u_L = 0.058$ m/s, $\epsilon = 0.83$, $d_p = 5.5$ mm, $D_c = 10$ cm.

fraction of velocity events occurring within each pixel is a good approximation of what might be the average solids volume fraction within the same pixel can a volumetric balance check be performed (see, for example, Lin et al., 1985). Calculated with eqs 12 and 13 along with the velocity occurrences distribution, the relative deviation of volumetric balance across core and sidewall areas in the FDR was 27.8% and 23.8% for the glass beads and the PVC particles, respectively. The discrepancies indicate that a proper formulation of the balance equation should incorporate the $\epsilon_S(r)$ radial profile. It is noteworthy that the discrepancies found in this work fell well within the deviation range reported by Moslemian (1987) during his study of the motion of 625−800 μm glass beads in gas fluidized beds using a similar radioactive particle tracking technique. This author performed a continuity check of the balance equation through cylindrical shells as well as horizontal slices over the whole bed, including both bed ends and FDR, and found deviations between 1% and 44.5%.

Concluding Remarks

The motion of solids in liquid fluidized beds is an outcome of advective and dispersive effects, whose relative impact depends on particle size and density. A noninvasive radioactive particle tracking technique provided information on the 3-D particle trajectory, the axial and transverse dispersion coefficients, mean flow pattern, averaged velocities, and turbulent parameters (root-mean-square velocities, shear stress, turbulence intensity, etc.) in monolayer three-dimensional liquid fluidized beds of 5.5 mm poly(vinyl chloride) (less dense particles) and 3 mm glass beads (more dense particles).

From the analysis of the particle flow pattern and turbulent parameters in the fully developed region of the bed, the flow structure consisted of a core and an annulus in which the solids underwent distinct upward and downward movements. In each zone the solids vertical motion can be described using an axially-dispersed plug flow, while the radial motion can be described using a convectionless dispersion model.

In the fully developed region, radial rms velocities far outweighed average radial velocities, and therefore a dispersion-type mechanism solely accounted for solids displacements radially. Axial velocity profiles were bell-shaped, but the low-density particles rose in the bed core and descended in the wall region whereas the high-density particles descended in the bed core and rose in the wall region. Turbulence intensities were always greater than 1, and the low-density particles exhibited less anisotropy than the high-density particles.

So far, the results have been obtained under a limited range of experimental conditions, and it is desirable to deepen our understanding of solids motion phenomena in liquid fluidized beds using finer particles, multilayer fluidized beds, low-density particles, different distributor designs and column diameters, a wider range of bed porosities, and liquids other than water. RPT proved to be promising in describing the kinematics of solids in binary mixtures before and after the so-called layer inversion (Larachi et al., 1995), and a lot of work remains to be done on this front.

Acknowledgment

The authors gratefully acknowledge the financial support from the Natural Sciences and Engineering Research Council of Canada and the Fonds pour la Formation de Chercheurs et l'Aide à la Recherche du Québec.

Notations

AC = anisotropy coefficient
D = dispersion coefficient, mm^2/s
D_c = column diameter, cm
d_p = particle diameter, mm
I = turbulence intensity
Q = volumetric flow rate, mm^3/s
P = number of occurrences per compartment
r = radial position, mm
t = time, s
T = sample period, s
$\mathbf{u}$ = instantaneous Eulerian velocity vector, mm/s
u' = root-mean-square particle velocity, mm/s
$\langle \mathbf{u} \rangle$ = local ensemble-averaged Eulerian velocity vector, mm/s
U = time, azimuthal, and longitudinal averaged particle velocity, mm/s
$\langle u_k' u_l' \rangle$ = correlation between fluctuating Eulerian velocity components, mm^2/s^2
u_L = liquid fluidization velocity, m/s
$\langle \overline{X^2(\Xi,t)} \rangle$ = mean-square displacement, mm^2
x, y, z = Cartesian coordinates, mm

Greek Letters

ϵ = bed porosity
ϵ_S = average local solids volume fraction
θ = polar angle, deg
Ξ = point of release
ζ = reduced radius, r/column radius

Subscripts

c = core
FR = flow reversal
m = assigned to midpoint
r = radial
sw = sidewall
w = wall
z = axial
x, y = transverse

Acronyms

1-, 2-, 3-D = one, two, three-dimensional
AB = acetate bead
CARPT = computer-aided radioactive particle tracking
FDR = fully developed region

GB = glass beads
PVC = poly(vinyl chloride)
RPT = radioactive particle tracking
rms = root mean square

Literature Cited

Al-Dibouni, M. R.; Garside, J. Particle Mixing and Classification in Liquid Fluidised Beds. *Trans. Inst. Chem. Eng.* **1979**, *57*, 94.

Asif, M.; Kalogerakis, N.; Behie, L. A. Hydrodynamics of Liquid Fluidized Beds Including the Distributor Region. *Chem. Eng. Sci.* **1992**, *47*, 4155.

Bascoul, A.; Couderc, J. P.; Delmas, H. Mouvement des particules solides en fluidisation liquide−solide (Solids Movements in Liquid−Solid Fluidization). *Chem. Eng. J.* **1993**, *51*, 135.

Carlos, C. R.; Richardson, J. F. Solids Movement in Liquid Fluidized Beds−I Particle Velocity Distribution. *Chem. Eng. Sci.* **1968**, *23*, 813.

Cassanello, M.; Larachi, F.; Marie, M.-N.; Guy, C.; Chaouki, J. Experimental Characterization of the Solid Phase Chaotic Dynamics in Three-Phase Fluidization. *Ind. Eng. Chem. Res.* **1995**, *34*, 2971.

Degaleesan, S. Liquid Mixing and Turbulence in Bubble Columns. D.Sc. Thesis, Washington University, St. Louis, MO, 1997.

Degaleesan, S.; Roy, S.; Kumar, S. B.; Duduković, M. P. Liquid Mixing Based on Convection and Turbulent Dispersion in Bubble Columns. *Chem. Eng. Sci.* **1996**, *51*, 1967.

Degaleesan, S.; Duduković, M. P.; Toseland, B. A.; Bhatt, B. L. An Improved Mixing Model for Slurry Bubble Column Reactors. *Ind. Eng. Chem. Res.* **1997**, *36*, in press.

Devanathan, N.; Moslemian, D.; Duduković, M. P. Flow Mapping in Bubble Columns Using CARPT. *Chem. Eng. Sci.* **1990**, *45*, 2285.

Di Felice, R. Hydrodynamics of Liquid Fluidisation. *Chem. Eng. Sci.* **1995**, *50*, 1213.

Gbavčić, Z. B.; Vuković, D. V.; Zdanski, F. K. Tracer Particle Movement in a Two-Dimensional Water-Fluidized Bed. *Powder Technol.* **1990**, *62*, 199.

Godfroy, L.; Larachi, F.; Kennedy, G.; Chaouki, J. Simultaneous Measurement of the 3-D Position and Velocity of a Single Radioactive Particle in a CFB Riser at High Velocity. Proceedings of CFB V, Beijing, China, May 28−June 1, 1996; Paper MI2, pp MI2-1 and MI2-6.

Handley, D.; Doraiswamy, A.; Butcher, K. L.; Franklin, N. L. A Study of the Fluid and Particle Mechanics in Liquid-Fluidised Beds. *Trans. Inst. Chem. Eng.* **1966**, *44*, T260.

Hanratty, T. J.; Latinen, G.; Wilhelm, R. H. Turbulent Diffusion in Particulately Fluidized Beds of Particles. *AIChE J.* **1956**, *2*, 372.

Juma, A. K. A.; Richardson, J. F. Segregation and Mixing in Liquid Fluidized Beds. *Chem. Eng. Sci.* **1983**, *38*, 955.

Kang, Y.; Nah, J. B.; Min, B. T.; Kim, S. D. Dispersion and Fluctuation of Fluidized Particles in a Liquid−Solid Fluidized Bed. *Chem. Eng. Commun.* **1990**, *97*, 197.

Kmieć, A. Particle Distributions and Dynamics of Particle Movement in Liquid−Solid Fluidized Beds. *Chem. Eng. J.* **1978**, *15*, 1.

Larachi, F.; Kennedy, G.; Chaouki, J. A γ-Ray Detection System for 3-D Particle Tracking in Multiphase Reactors. *Nucl. Instrum. Methods Phys. Res., Sect. A* **1994**, *338*, 568.

Larachi, F.; Lord, E.; Chaouki, J.; Chavarie, C.; Behie, L. A. Phenomenological Study of Solids Mixing in a Binary Liquid Fluidized Bed. Proceedings of Fluidization VIII, Tours, France, 1995; pp 385−392.

Larachi, F.; Cassanello, M.; Chaouki, J.; Guy, C. Flow Structure of the Solids in a Three-Dimensional Gas−Liquid−Solid Fluidized Bed. *AIChE J.* **1996**, *42*, 2439.

Latif, B. A. J.; Richardson, J. F. Circulation Patterns and Velocity Distribution for Particles in a Liquid Fluidised Bed. *Chem. Eng. Sci.* **1972**, *27*, 1933.

Limtrakul, S. Hydrodynamics of Liquid Fluidized Beds and Gas−Liquid Fluidized Beds. D.Sc. Thesis, Washington University, St. Louis, MO, 1996.

Lin, J. S.; Chen, M. M.; Chao, B. T. A Novel Radioactive Particle Tracking Facility for Measurement of Solids Motion in Gas Fluidized Beds. *AIChE J.* **1985**, *31*, 465.

Mandelbrot, B. B.; Wallis, J. R. Computer Experiments with Fractional Gaussian Noises. Part 2, Rescaled Ranges and Spectra. *Water Resour. Res.* **1969**, *5*, 242.

Monin, A. S.; Yaglom, A. M. In *Statistical Fluid Mechanics: Mechanics of Turbulence*; Lumley, J. L., Ed.; MIT Press: Cambridge, MA, 1971; Vol. 1.

Moslemian, D. Study of Solids Motion, Mixing, and Heat Transfer in Gas-Fluidized Beds. Ph.D. Thesis, University of Illinois, Urbana−Champaign, IL, 1987.

Roy, D.; Larachi, F.; Legros, R.; Chaouki, J. A Study of Solid Behavior in Spouted Beds Using 3-D Particle Tracking. *Can. J. Chem. Eng.* **1994**, *72*, 945.

Volpicelli, G.; Massimila, L.; Zenz, F. A. Non-Homogeneities in Solid−Liquid Fluidization. *Chem. Eng. Prog. Symp. Ser.* **1966**, *62*, 42.

Received for review February 16, 1997
Revised manuscript received August 27, 1997
Accepted August 27, 1997[⊗]

IE970161K

[⊗] Abstract published in *Advance ACS Abstracts*, October 15, 1997.